EBioMedicine 39 (2019) 562–574

Contents lists available at ScienceDirect

EBioMedicine

journal homepage: www.ebiomedicine.com

EBioMedicine
Published by THE LANCET

# Medium- to long-term survival and functional examination of human iPSC-derived retinas in rat and primate models of retinal degeneration

Hung-Ya Tu [a,1], Takehito Watanabe [a,b,1], Hiroshi Shirai [a,c,1], Suguru Yamasaki [a,d,e,1], Masaharu Kinoshita [f], Keizo Matsushita [a,e], Tomoyo Hashiguchi [a], Hirotaka Onoe [g], Take Matsuyama [a], Atsushi Kuwahara [d,e], Akiyoshi Kishino [d,e], Toru Kimura [d,e], Mototsugu Eiraku [h], Kiyoshi Suzuma [b,i], Takashi Kitaoka [b], Masayo Takahashi [a], Michiko Mandai [a,j,*]

[a] Laboratory for Retinal Regeneration, RIKEN Center for Biosystems Dynamics Research, Kobe 650-0047, Japan
[b] Department of Ophthalmology and Visual Science, Graduate School of Biomedical Science, Nagasaki University, Nagasaki 852-8501, Japan
[c] Department of Ophthalmology, Nagoya University Graduate School of Medicine, Nagoya 466-8550, Japan
[d] Regenerative and Cellular Medicine Kobe Center
[e] Regenerative and Cellular Medicine Office, Sumitomo Dainippon Pharma Co., Ltd., Kobe 650-0047, Japan
[f] Department of Physiology, Hirosaki University School of Medicine, Hirosaki 036-8562, Japan
[g] Human Brain Research Center, Kyoto University Graduate School of Medicine, Kyoto 606-8501, Japan
[h] Laboratory of Developmental Systems, Institute for Frontier Life and Medical Sciences, Kyoto University, Kyoto 606-8507, Japan
[i] Department of Ophthalmology and Visual Sciences, Kyoto University Graduate School of Medicine, Kyoto 606-8501, Japan
[j] RIKEN Program for Drug Discovery and Medical Technology Platforms (DMP), Yokohama 230-0045, Japan

ARTICLE INFO

*Article history:*
Received 6 August 2018
Received in revised form 1 November 2018
Accepted 14 November 2018
Available online 28 November 2018

*Keywords:*
Retinal degeneration
Human iPSC
Photoreceptor transplantation
Visually-guided saccades
Multi-electrode array

ABSTRACT

*Background:* We have previously reported that xeno-transplanted human ESC-derived retinas are able to mature in the immunodeficient retinal degeneration rodent models, similar to allo-transplantations using mouse iPSC-derived retina. The photoreceptors in the latter developed outer segments and formed synapses with host bipolar cells, driving light responses of host retinal ganglion cells. In view of clinical application, here we further confirmed the competency of human iPSC-derived retina (hiPSC-retina) to mature in the degenerated retinas of rat and monkey models.
*Methods:* Human iPSC-retinas were transplanted in rhodopsin mutant SD-Foxn1 Tg(S334ter)3LavRrrc nude rats and two monkeys with laser-induced photoreceptor degeneration. Graft maturation was studied by immunohistochemistry and its function was examined by multi-electrode array (MEA) recording in rat retinas and visually-guided saccade (VGS) in a monkey.
*Findings:* A substantial amount of mature photoreceptors in hiPSC-retina graft survived well in the host retinas for at least 5 months (rat) to over 2 years (monkey). In 4 of 7 transplanted rat retinas, RGC light responses were detected at the grafted area. A mild recovery of light perception was also suggested by the VGS performance 1.5 years after transplantation in that monkey.
*Interpretation:* Our results support the competency of hiPSC-derived retinas to be clinically applied for transplantation therapy in retinal degeneration, although the light responses observed in the present models were not conclusively distinguishable from residual functions of degenerating host retinas. The functional analysis may be further elaborated using other models with more advanced retinal degeneration.


## 1. Introduction

Transplantation therapy using retinal cells or tissues for treating retinal degeneration has been intensively studied for its potential as a promising cure, supported by the numerous reports on graft integration and visual function restoration [1–8], as well as the innovation on protocols for producing 3D-retinas from mouse and human embryonic stem cells/induced pluripotent stem cells (ESC/iPSCs) [9–11]. Transplanted photoreceptor precursors were recently suggested to act by supplying missing proteins to the remaining host photoreceptors *via* "material transfer" [12–14]. Therefore, the present consensus of the field for testing *de novo* synaptic reconstruction between the host

* Corresponding author.
*E-mail address:* michiko.mandai@riken.jp (M. Mandai).
[1] These authors equally contributed to this work.

https://doi.org/10.1016/j.ebiom.2018.11.028

**Research in context**

*Evidence before this study*

Possible restoration of visual function in the end-stage retinal degeneration rodent models by rodent and human fetus retinas and ES/iPSC-derived retinal tissues/cells have been suggested in past years. We have previously reported that allo-transplantaion of mouse ES/iPSC-retinas can develop structured photoreceptor layer after transplantation and drive light responses in the end-stage retinal degeneration retinas with few remaining photoreceptors. We also reported that xeno-transplanted human ESC-derived retinas mature in the immunodeficient end-stage retinal degeneration models of rodents and monkeys, and can recover light responses in a mouse model but of less robustness compared to allo-transplantation. These studies imply the competency of humen ESC-derived retinas but also leave the difficulties in obtaining functional data from xeno-transplantation of neural tissues/cells where reconstruction of host-graft neural network is required. Since the use of iPS cells would allow for the application of cell therapy by overcoming the ethical/religious issues as well as for the use of varieties of choices of cell lines such as HLA-matched iPSC cell lines, the examinations for competency of iPSC-retina as graft source was of great importance in view of clinical application.

*Added value of this study*

This study provided the evidence to show human iPSC-derived retinas have histological and physiological properties that are consistent with human ESC-derived retinas and are competent as a graft source by providing fully mature photoreceptors in organized layers in both of rat and monkey models. Mildly better light responses were suggested at the grafted areas in 2 different animal models - in rats compared to the age-matched non-transplanted controls, and in one monkey model after 1.5 years of transplantation, although the graft driven light responses were not conclusively distinguishable from the remaining light sensitivity of the host retina. Over 2-year survival of substantial amount of photoreceptor cells in hiPSC-retina graft in the primate model also complies with competency for clinical use.

*Implications of all the available evidence*

Although evident recovery of visual function originated from the graft was undetermined by xeno-transplantation with the current animal models, the present study suggested the consistent competency of human iPSC-derived retina to human ES-derived retinas with substantial survival period. Our results are relevant to show the feasibility of human iPSC-retinas in clinical application of transplantation therapy, where functional integration of neural cells/tissues should after all be tested in human clinical trials. The present study using monkey models also provides insights into what we can possibly expect and how we can monitor the post-operative courses of hiPSC-retina transplantation in human application.

and graft cells is the use of end-stage degeneration retina with minimal remaining photoreceptors, which would also be the case of the very first clinical application of retinal transplantation in the future.

In Retinitis Pigmentosa (RP), rod photoreceptors gradually perish and the "ONL-absent area" expands from midperiphery toward central areas over decades, subsequently leading to the loss of central cone photoreceptors as the secondary pathological change in advanced RP cases [15,16]. The transplantation efficacy of photoreceptor progenitor suspension cells differentiated from hESC/iPSC in the end-stage degenerative retina was reported by Barnea-Cramer, Wang [6] while we have confirmed the feasibility of ESC/iPSC-retinal sheet transplantation in the end-stage models of retinal degeneration. Structured ONL composed of mature photoreceptors with outer segment structure was consistently observed by electron microscopy in the transplanted miPSC- and hESC-retinas [5,7,8]. Synaptic formation between the host bipolar cells and graft photoreceptors was confirmed by immunohistochemistry along with light sensitivity detected by multi-electrode array (MEA) recordings in both allo- and xeno-transplantation preparations using miPSC- and hESC-retinas, respectively [8,17]. While the functional recovery was also supported by light perception shown by behavior test in the miPSC allo-transplantation [17], the *de novo* light response of hESC xeno-transplantation preparation detected by electrophysiology recording was less robust [8]. The competency of functional integration of human stem cell-derived retinas in human retinal degeneration, therefore, has to be tested in the future clinical trials in form of allo-transplantation.

Recently, the advantages of Human Leukocyte Antigen (HLA)-matched iPSCs were reported to reduce the risk of rejections [18,19] and some populations also favor the use of graft tissue/cell from iPSCs than ESCs for ethical or religious reasons. In this study, we first demonstrated the maturation of hiPSC-retinas transplanted to rhodopsin mutant SD-Foxn1 Tg(S334ter)3LavRrrc nude rats, consistent with our previously reported hESC-retina preparation. Five of 7 retinas showed some light responses at the graft site. We further assessed the long-term graft survival and visual function in a monkey retinal degeneration model by the visual field test. Mild recovery of light perception was suggested associated with the grafted area >1 year after transplantation, wherein structured graft photoreceptor cells were confirmed to survive for over 2 years. Our results support the feasibility of the use of hiPSC-retinas in clinical application.

## 2. Materials and methods

### 2.1. Animals

All animals were treated in accordance with the Association for Research in Vision and Ophthalmology statement for the use of Animals in Ophthalmic and Vision Research. Animal experiments were conducted with the approval of the Animal Research Committee at RIKEN Center for Developmental Biology (now Center for Biosystems Dynamics Research). As described previously [7], the SD-Foxn1 Tg(S334ter) 3LavRrrc nude rats [20] were obtained from the Rat Resource and Research Center and the 2 monkeys were obtained from Shin Nippon Biomedical Laboratories and Japan Bio Science Center, respectively. All animals were housed under the standard 12-h light/dark cycle.

For laser photocoagulation, *in vivo* imaging, head holder implantation, and iPSC-retina transplantation, the monkeys were first anesthetized with intramuscular injection of ketamine hydrochloride (10 mg/kg) and xylazine (2 mg/kg), followed by a periodic additional ketamine hydrochloride (5 mg/kg) and xylazine (1 mg/kg) for approximately every 30 min to maintain the anesthesia state when necessary. For iPSC-retina transplantation in rats, the animals were anesthetized with ketamine hydrochloride (40–80 mg/kg) and xylazine (5–10 mg/kg), or by inhalation of 3–5% isoflurane. Pupils were dilated with 0.5% tropicamide and 0.5% phenylephrine hydrochloride, and tropical 1% tetracaine or 0.4% Oxybuprocaine Hydrochloride was used for cornea anesthetization when needed.

### 2.2. Human iPSC differentiation

Human iPSC-1231A3 line was established by Kyoto University, derived from ePBMC (Cellular Technology Limited; http://www.immunospot.com/) [21]. Human iPSCs were maintained on LM511-E8

**Table 1**
Summary of examined transplanted nude rat eyes.

| Eye | hiPSC-retina at transplantation[1] | hiPSC-retina at examination[1] | Transplantation ~ Examination | | Examination |
|---|---|---|---|---|---|
| | | | Rat age[2] | Duration[2] | |
| IHC_01 ~ 08 | DD58 | DD317 | 2.5 M ~ 11 M | 8.5 M | Immunohistochemistry |
| IHC_09 ~ 11 | DD66 | DD353 | 3.5 M ~ 13 M | 9.5 M | Immunohistochemistry |
| MEA_01 | DD58 | DD210 | 5.5 M ~ 10.5 M | 5 M | MEA recording |
| MEA_02 | DD58 | DD226 | 5.5 M ~ 11 M | 5.5 M | MEA recording (Fig. S4) |
| MEA_03 | DD58 | DD226 | 5.5 M ~ 11 M | 5.5 M | MEA recording |
| MEA_04 | DD58 | DD229 | 5 M ~ 10.5 M | 5.5 M | MEA recording (Fig. 2) |
| MEA_05 | DD58 | DD229 | 5 M ~ 10.5 M | 5.5 M | MEA recording (Fig. 3) |
| MEA_06 | DD78 | DD368 | 2 M ~ 12 M | 10 M | MEA recording (Fig. S4) |
| MEA_07 | DD78 | DD396 | 2 M ~ 12.5 M | 10.5 M | MEA recording (Fig. S4) |

[1] DD, differentiation day.
[2] M, month.

matrix (Nippi) in StemFit medium (Ajinomoto) according to the published protocol [21]. The differentiation to retinal tissue was conducted following the culture methods designated SFEBq, BMP and Induction-reversal culture described previously [10] with minor modification at the initial phase in differentiation (Kuwahara et al., in submission). Human iPSC-retinas at differentiation day (DD) 58–78 were cut into small pieces of approximately 0.5 × 2 to 1 × 1.5 $mm^2$ for transplantation.

### 2.3. Transplantation into nude rats

Human iPSC-derived retinal sheets were inserted into subretinal space of SD-Foxn1 Tg(S334ter)3LavRrrc nude rats aged from 2 to 5 months using glass pipettes as previously described [5]. Transplanted rats were sacrificed for retina harvest after 5 to10 months for immunohistochemistry and acute electrophysiology recording as summarized in Table 1.

### 2.4. Multi-electrode array (MEA) recordings

The nude rats used for MEA recording were dark-adapted for 1–3 days prior to retina harvest and recording, following the similar procedures for mouse retina recording with both MED64 system (Alpha MED Scientific Inc.) and USB-MEA60-Up-System (MultiChannel Systems, Germany) reported previously [8]. In brief, under dim red light peaked at 690 nm, the animals were deeply anesthetized by intramuscular injection of the ketamine-xylazine mixture, and euthanized by sevoflurane inhalation immediately after enucleation. The eyecups were carefully washed and incubated with constantly oxygenated Ames' medium (A1420, Sigma-Aldrich) in the dark at room temperature before use. After removing the vitreous body, the freshly isolated retina was trimmed to a degree that both optic nerve disc and mid-peripheral regions were retained, including the potentially grafted areas, before mounting on the electrodes (MED-P515A for MED64 system; 60MEA200/30iR-Ti-gr for MEA60 system) with the retinal ganglion cell (RGC) side down. Note that since the transplanted hiPSC-retinal sheets were not engineered for any fluorescence labeling, the grafted areas were targeted by identifying the whitish spotted regions in between the optic nerve disc and the entry holes made during transplantation. IR-DIC images of retinas mounted on electrodes were taken during and after recording to determine the correlation of electrodes and grafts with Recoverin and/or STEM121 immunoreactivity afterwards.

The recording was conducted with constant perfusion of warm, oxygenated Ames' medium (34–35 °C) at 3–3.5 mL/min. Opsinamide (10 μm; AA92593, Sigma-Aldrich) was contained in the perfusion medium from the beginning to suppress the intrinsic photosensitivity of melanopsin-expressing ganglion cells. Retinas were allowed to recover in the MEA chamber for >20 min before recording while monitoring the spontaneous RGC firing as the feature of degenerating retina. Full-field light stimuli ranging from 10 to 13 log photons/$cm^2$/s were generated with a white LED source as reported previously to cover the low to the high mesopic range [8]. Field potentials were recorded for a 10-s duration to reveal the micro-ERG (mERG) b-waves to 10-ms stimuli; RGC action potentials to 1-s light stimuli were recorded for a 21-s duration and sorted offline (Spike2, Version 7.20, CED) to separate individual cells with spikes. We categorized the detected RGCs to spontaneous firing, ON/OFF/ON-OFF/Delayed-ON light response types, or hypersensitive type automatically, based on their temporal spiking pattern corresponding to the light stimulus onset and offset using the homemade R scripts. Recordings to the same set of light stimuli were repeated before, during and after the L-AP4 application (10 μm; 016–22083, Wako), for which blocks the metabotropic glutamate receptor type 6 (mGluR6)-mediated photoreceptor-ON bipolar cell transmission, to confirm the photoreceptor-origin of detected light responses. The retinas were detached from the electrodes after recording and fixed with 4% paraformaldehyde (PFA) at room temperature for immunostaining and confocal imaging.

### 2.5. Monkey model preparation

Parts of the ONL in the peri-macular regions were ablated focally in single eyes of a cynomolgus monkey (*Macaca fascicularis*) and a rhesus monkey (*Macaca mulatta*) aged at 8 and 6 years old, respectively, using the 577-nm OPSL PASCAL laser system (Topcon Medical Laser Systems) under anesthesia as described previously [7]. In brief, 16 laser spots (4 × 4) of 100 μm diameter with 0-μm interval setting were applied simultaneously for a pulse duration of 15 ms triggered by a single foot pedal depression. To induce selective ONL damage, "barely visible" grade laser photocoagulation was first applied as a trial pulse and the resulted lesion was evaluated by direct fundus observation and optical coherence tomography (OCT) imaging (RS-3000; NIDEK) immediately after the trial. Once the optimal laser power was determined, the selected regions were then targeted for continuous laser treatment to generate the degeneration model areas.

### 2.6. Transplantation to monkey models

We previously monitored the stability of the monkey ONL depletion models up to 7 months by laser photocoagulation or cobalt chloride subretinal injection, in which we transplanted hESC-retinas to these primate models at 1.5 to 3.5 months after ONL ablation and reported the time-dependent maturation of the grafts [7]. In the present study, therefore, we conducted hiPSC-retinas transplantation about 2 months after the laser photocoagulation (62 days for the cynomolgus monkey and 53 days for the rhesus monkey). In brief, following the vitrectomy, intraocular irrigating solution (BSS Plus; Alcon) was slowly injected to make a subretinal space in the degenerated area and the graft insertion site was carefully enlarged by scissors, along with the creation of retinotomy site for subretinal fluid drainage. Grafts were placed into the subretinal space of degenerative regions using the outer tube of a 24-gauge

indwelling needle (Terumo), followed by subretinal fluid drainage with perfluorocarbon liquid (Alcon). After the fluid-air exchange, silicon oil (Alcon) was injected into the eye, which was removed 13 months after transplantation. The immunosuppressant Cyclosporine (Sigma-Aldrich) was administered throughout the observation period starting from 3 days prior to transplantation by daily intravenous injection on weekdays (5 times per week) at an initial dose of 20 mg/kg per day. The serum levels were monitored monthly for dose adjustment to achieve 70–200 ng/mL concentration (see also Fig. S6). The transplanted eyes were routinely monitored under anesthesia using fundus cameras (CX-1, Canon; RetCam, Clarity) with and without the fluorescein angiography (FA), and also examined with OCT (RS-3000; NIDEK) at 1 and 2 weeks post-operation, followed by monthly check afterwards.

### 2.7. Monkey visual field test

The visual function of the transplanted eye of the rhesus monkey was assessed by monitoring its visually-guided saccades (VGS) onto target spots displayed on a colour LCD monitor (Dell 1704FPVt; 1024 × 768 pixels) placed 31.2 cm in front of its face as previously described [22,23]. Two weeks before the VGS training began, the monkey was implanted with a head holder under anesthesia to control its face position during VGS tests. The experiment was conducted in dark to evaluate both rod and cone visions, and the eye movements were tracked by a high-speed CMOS image sensor (C8201, Hamamatsu Photonics). The monkey was first trained to fixate on a central fixation spot (displayed randomly for 400–1200 ms) followed by the random presentation of a target spot (0.15 cd/m$^2$) somewhere else in the monitor (gray background, 0.90 cd/m$^2$). The monkey was deprived of drinking water from the night before test and was rewarded with a drop of water for every correct eye movement defined as a single saccade to the presented target with maintained gaze fixation for >200 ms. Saccades falling in a square of 50 × 50 pixels around the visual target were judged as correct responses. To unbiasedly map the visual field, in each test session a series of target points would be randomly generated from a defined set of target choices, which differed from each other in direction and/or distance to the fixation spot. Each chosen point would be tested for 4–8 times in a randomized order, resulting in approximately 250 targets tested in a day as one session. The correct response ratios for all tested positions were calculated for each day and were averaged after the completion of 4–8 sessions as one test period spanning around one month. Four periods of visual field tests were conducted before the laser injury, before transplantation, approximately 1 year (as the first post-operation period) and 1.5 years after transplantation (as the second post-operation period), respectively.

### 2.8. Focal ERG recording

Focal electroretinogram (ERG) recording was done with Neuropack MEB-9402 Measuring System (Nihon Kohden) using the Burian–Allen Bipolar ERG Electrodes (Hansen Ophthalmic Development Laboratory) and a ground electrode attached on the ear. An ER-80 Visual Stimulator (Kowa) was used to elicit focal ERGs with light spot size at 10° and repetition rate at 2 Hz. Recordings were band-pass filtered between 5 and 500 Hz and averaged over 200 repeats.

### 2.9. Immunohistochemistry

The hiPSC-derived 3D retinas and freshly harvested rat eyes were fixed with 4% PFA, cryoprotected with 30% sucrose in PBS overnight at 4 °C, embedded in OCT compound (Tissue Tec; Sakura Finetek Japan) and sectioned at 12-μm thickness using a cryostat (CM3050S; Leica). The transplanted eye of the cynomolgus monkey was fixed with SUPERFIX (Kurabo) followed by automatic dehydration (Excelsior; ThermoFisher Scientific), paraffin embedding (P3683; Sigma-Aldrich) and sectioned at 10-μm thickness using the AS-200 Auto Slide Preparation System (Kurabo). The rhesus monkey eye with hiPSC-retina transplantation was freshly isolated from the eyecup, fixed in 4% PFA, and the piece of retina centered with the graft was cut out for flat-mount immunostaining, followed by cryo-section at 12-μm thickness. Both vertical sections and flat-mount preparation were processed for immunostaining following the procedures described previously [5,8,24]. The primary antibodies and dilution factors are summarized in Table S1. Cell nuclei were counterstained with 4′,6-diamidino-2-phenylindole (DAPI; 1 μg/mL, Molecular Probes). Labeled samples were mounted with VECTASHIELD mounting medium (Vector Laboratories) and kept in dark at 4 °C before imaging with Zeiss LSM700 and Leica-TCS SP8 confocal microscopes.

## 3. Results

### 3.1. Competency of human iPSC-retina for transplantation and maturation in rat retinal degeneration model

We first tested if hiPSC-derived retina can integrate and develop structured ONL with functional photoreceptors as we previously reported with hESC-retina, in which hESC-retina of any developmental stage between DD50 and DD150 showed maturation over DD200 [7]. Human iPSCs could be consistently differentiated into optic vesicles, expressing Collagen IV on the basal side and Ezrin and PKCζ on the apical side at DD58 (Fig. S1a-b). These iPSC-retinas were mainly composed of Chx10- and/or Pax6-positive retinal progenitor cells (Fig. S1c). Islet1-positive inner retinal neuron precursors, including Brn3-positive retinal ganglion cells, were found mostly in the basal half while differentiating Prox1-positive cells were mainly seen in the apical half (Fig. S1d-e). The apical side was characterized by rows of Crx-positive (photoreceptor marker) cells, some of which showed rudimentary photoreceptor morphology with Recoverin expression (Fig. S1f), and most of which showed expression of cone precursor marker RxRγ (Fig. S1g) indicating cone genesis.

SD-Foxn1 Tg(S334ter)3LavRrrc nude rats are immune-deficient progressive retinal degeneration model rats that express a mutant rhodopsin mimicking human retinitis pigmentosa (RP) of dominant inheritance [20]. This rat model is reported with a rapid loss of rod photoreceptors and only a few rods remain by 10 weeks after birth, therefore the hiPSC-retinas at around DD60 were transplanted to 2.5 to 3-month-old SD-Foxn1 Tg(S334ter)3LavRrrc nude rats. The consistent medium-term survival and maturation of the graft were confirmed 8–9 months later ($n = 11$ eyes; summarized in Table 1) by immunohistochemistry (Fig. 1). Human-origin graft cells were restrained at the transplantation site (Fig. 1a and g) as indicated by the human nuclei (Ku80) and cytoplasm (STEM121) markers. Graft photoreceptors formed rosettes, which were capable of forming outer segments as indicated by the expression of Rhodopsin, Peripherin-2 and cone opsins (Fig. 1a-b). Chx10-, Pax6- and Islet1-positive inner retinal neurons of graft origin (indicated by human nuclei marker HuNu or Ku80) were sometimes observed in the host inner nuclear layer (INL), implying the migration of graft bipolar and amacrine cells, although Brn3-positive graft retinal ganglion cells (RGCs) were rarely observed (Fig. 1c). The integration of graft inner neurons was also observed by the colocalization of STEM121, and PKCα staining in the host INL and IPL (Fig. 1g), likely to be the human rod bipolar cells with their human origin suggested by Ku80 in the nuclei. Some of the PKCα-positive host rod bipolar cells were found with extended dendrites toward the rosettes, potentially making synaptic contact with graft photoreceptors (Fig. 1d), while their axons remained in the host inner plexiform layer (IPL).

The potential synaptic connections between host bipolar cells and graft photoreceptors were further indicated by the expression of the presynaptic Ribeye proteins in apposition to host bipolar cell dendritic tips (Fig. 1e-e'). In addition to the conventional chemical synapses, we also probed the expression of connexin 36 (Cx36) as the most representative gap junction protein type in both the outer plexiform layer (OPL) among photoreceptors and the proximal IPL, contributed largely by AII amacrine cells [25]. Cx36 puncta were abundantly expressed in the

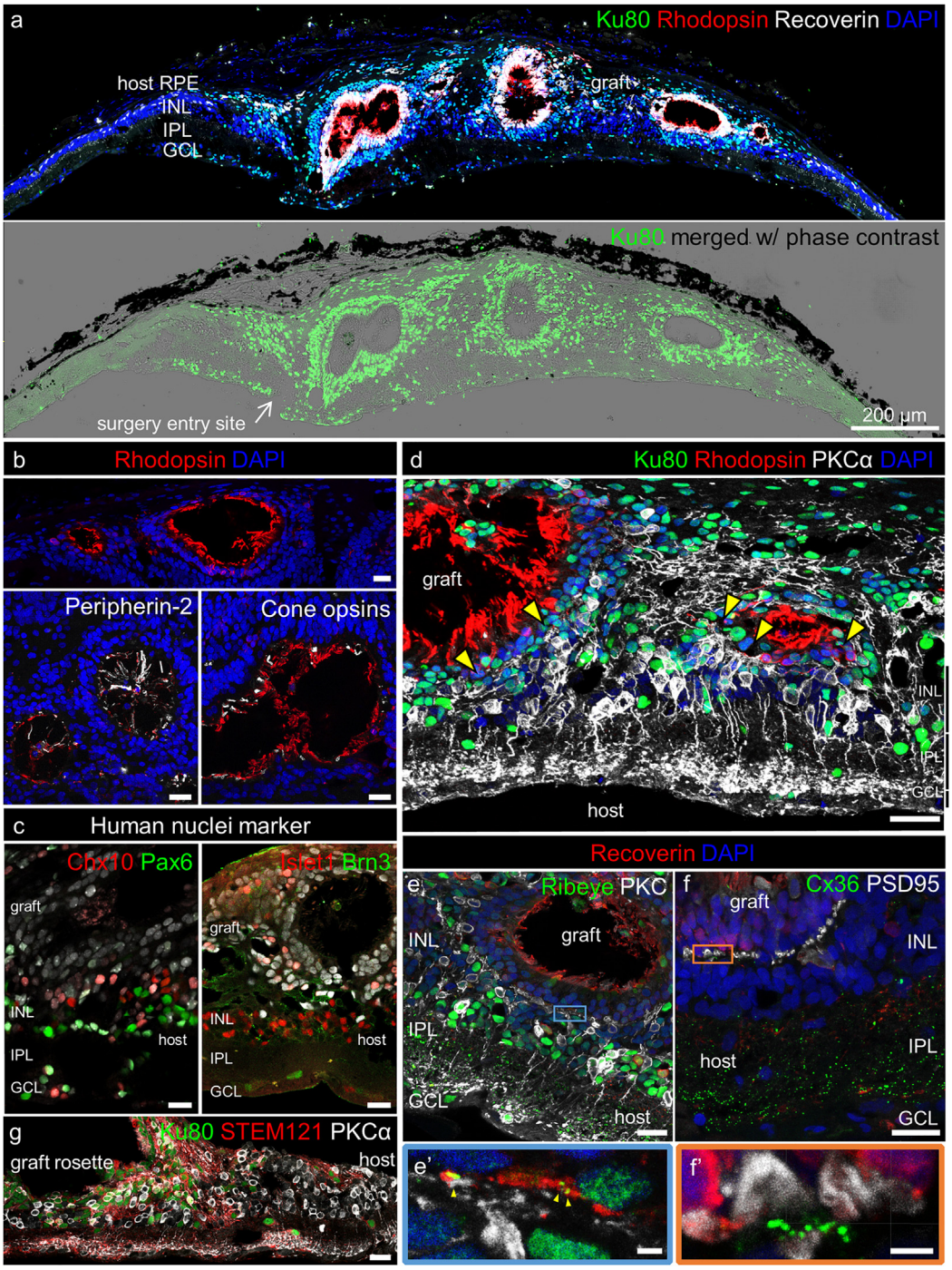


**Fig. 1.** Maturation and integration of hiPSC-retina after sub-retinal transplantation in SD-Foxn1 Tg(S334ter)3LavRrrc nude rats. (a) Rosettes formed with Recoverin- and Rhodopsin-positive graft photoreceptors of the transplanted human iPSC-retina in the host subretinal space. Human origin cells with Ku80-positive nuclei were confined to the close proximity to the transplantation site. (b) Maturation of graft photoreceptors with inner and outer segment formation indicated by the expressions of Rhodopsin, Peripherin-2 and cone opsins (c) Migration of Chx10-, Pax6-, or Islet1-positive graft-origin inner retinal neurons, presumably bipolar and amacrine cells but not ganglion cells marked by Brn3, into the host INL/IPL. (d) Potential contacts found between the dendritic tips of extending PKCα-positive host rod bipolar cells with Rhodopsin-positive graft photoreceptors. (e-f) Ribbon synapse (e) and Cx36 gap junction (f) formation at the graft photoreceptor axon terminals. Note that both expressions of Ribeye and Cx36 were also found in the host IPL, suggesting the normal signal transmission in the host inner retina. Magnified views of the blue and orange boxes were shown in (e') and (f'), respectively, showing the Ribeye and Cx36 protein expressions by the graft photoreceptors at the host-graft interface. (g) One example of the limited migration of graft cells at the graft-host interface, where PKCα-positive rod bipolar cells of both human (Ku80-positive nuclei wrapped with STEM121-positive cytoplasm) and rat origins were observed. GCL, ganglion cell layer; IPL, inner plexiform layer; INL, inner nuclear layer; ONL, outer nuclear layer. Scale bars equal to 200 μm (a), 20 μm (b-g) and 2 μm (e', f').

proximal IPL of hiPSC-retina transplanted nude rat retinas (Fig. 1f) and also surrounding the graft photoreceptor terminals marked by PSD95 staining (Fig. 1f'). Cx36 gap junctions found among graft rods and cones may contribute to electrical transmission inside the rosettes and thus the amplification of graft photoreceptor light responsiveness.

### *3.2. Light responses of degenerative rat retina after hiPSC-retina transplantation*

To identify the graft-driven light responses in transplanted nude rat retinas, we first tested the remaining photosensitivity of SD-Foxn1 Tg

(S334ter)3LavRrrc rat retinas at different ages (Fig. S2). Although the S334ter line-3 transgenic rat model showed relatively fast degeneration progress with almost no ONL structures observed by postnatal day (P) 30, only 15–20% drop of the maximal cone response was reported at P30 and P60, followed by a rapid decrease becoming undetectable by P120 [26]. In fact, we still observed, in a 10-month-old nude rat retina, a few Rhodopsin- and/or Cone arrestin-positive cells with abnormal morphologies located at the INL apical surface (Fig. S2a and b), which were presumably photoreceptors and might explain the remaining light responses of RGCs detected in nude rat retinas younger than 6 months old in our multi-electrode array (MEA) recording (Fig. S3). However, the residual light response drastically dropped in nude rats aged around 1 year. Therefore in the present study, we tested both the transplantation of iPSC-retinas (DD58 and DD78, see also Table 1) in 2- and 5-month-old nude rats and light responses were recorded at 10–12 months of age when remaining light responses were scarcer (Figs. 2, 3 and S4). The recordings were made at the central retinal region proximal to the optic nerve disc, where the grafts could be identified by their characteristic appearance under IR-DIC observation (Fig. 2b and 3b; see also Materials and methods). The graft positions on the MEA electrodes were confirmed again by corresponding the IR-DIC images to the fluorescence images of flat-mount retinas stained against Recoverin and/or STEM121 after the recording (Fig. 2a, 3a and S4).

Total of 7 transplanted rat retinas were tested for light sensitivity by MEA recording. In 4 retinas we detected the L-AP4 sensitive RGC light responses to the 1-s full-field stimuli of 12.84 log photons/cm$^2$/s intensity, approximately corresponding to the mesopic-to-photopic light level (Fig. 2 and S4). A few clearly responding RGCs were detected in two of the 4 retinas 10 months after transplantation (12-month-old), and more prominent responses were observed in the other 2 retinas of late transplantation (5-month-old) at the proximal areas and showed a clear correlation to the graft positions (see also Table 1 for graft information). For one of the latter, the peri-stimulus time histograms (PSTHs) of averaged RGC spikes in response to 3 different light intensities were shown (Fig. 2c-d) in parallel with results from an age-matched (10-month-old) degenerated rat retina without transplantation (Fig. 2d, "Age-match control"). The RGC counts were categorized upon response types and mapped in correlation to the electrode position (Fig. 2c, lower row), showing the dominance of ON responses as one of the features we have been seeing in transplanted retinas of different species [8,17]. It is noteworthy that in this retina without hypersensitive responses, the occurrences of light responses and spontaneous firing were mutually exclusive in most channels, different from the control retinas within 6 months of age showing robust hypersensitive activities in addition to the coexistence of spontaneous firing and light responses (Fig.2c and S3a-d). RGC light responses to the two brighter stimuli (Fig. 2d and S3c) were also seen in the non-transplanted retina potentially with a few photoreceptors remained (see also Fig. S2). The responses to the dimmest light stimulation, however, were only detected in one of the transplanted retinas (Fig. 2d, left) but not in the control, suggesting the beneficial effect of hiPSC-retinal transplant.

Interestingly, small but uniform mERG b-waves were detected in one of the 3 retinas without RGC light response after transplantation, suggestive of the light responsiveness of the graft without host-graft connectivity (Fig. 3). The mERG responses to 10-ms full-field flash light stimuli were shown (Fig. 3c) in parallel with the field potential recordings from the same age-matched degenerated retina shown for residual RGC responses in Fig. 2. Note that different from the grafted retina (Fig. 3b, left), the recording of the age-matched control was done in mid-peripheral retina about 4 mm away from the optic nerve disc (Fig. 3b, right). There were no responses to our dimmest stimulation (10.56 log photons/cm$^2$/s) but noisy fluctuation of field potentials detected in both retinas (Fig. 3c, left-most). To the other 2 brighter stimuli, single upward peaks were seen in the transplanted retina, with a wave-like spread-out from the central region. In contrast, in the control large downward peaks followed by rebounding upward peaks were found in some channels (Fig. 3c) where L-AP4 dependent RGC responses were detected as shown in Fig. 2, suggesting the downward peak components were considered as RGC depolarization and spiking activity. The sensitivity to L-AP4 indicates these mERG/field potential responses were originated from synaptic transmission from photoreceptors to ON bipolar cells. The responses to medium light stimulation in the boxed neighboring channels from both samples were magnified in Fig. 3d to demonstrate the similar latency between the "transplanted" upward peaks (marked with red dotted lines) and the "control" RGC firing (downward peaks). Moreover, nor RGC response or even spontaneous firing was detected in most of the channels with upward peaks (Fig. 3e). These results suggest the relatively slow upward peaks seen in the transplanted retina were originated from the graft ON bipolar cells, which were presumably distal from the host retina (and hence the electrodes) and may have physically hindered the formation of graft photoreceptor-host bipolar connection.

### 3.3. Maturation and integration of iPSC-retina in a monkey model of retinal degeneration

In parallel to the hiPSC-retina transplantation in nude rat models, two monkeys were prepared as the primate model with end-stage retinal degeneration following the protocol we previously described (see also Materials and methods) [7] and were dedicated to providing insightful observation for both morphological and functional integration potentials of hiPSC-retina transplants. In the first case, a piece of hiPSC-retina at DD63 was transplanted to the ONL-ablated region in a cynomolgus monkey eye about 2 months after focal laser photocoagulation in the peri-macular area (Fig. 4a-b). OCT image at 6 months post-operation shows the presence of rosette-like structures inside the graft (Fig. 4b). Similar to our previous report with hESC-retinas, the hiPSC-retina graft maturation in this monkey was histologically confirmed 7 months after transplantation (~DD282). Instead of the human nuclei markers used for the nude rat preparation, which are known to cross-react with non-human primate cells, the hiPSC-graft cells transplanted to monkey models were marked by STEM121 staining specific for human cytoplasm (Fig. 4c, e, and h; see also Fig. 6h and S5). Note that our observation of STEM121 specificity to human cytoplasm was consistent with the product information provided by the manufacturer. In the degenerated host retinas, Recoverin-positive photoreceptors of human origin formed rosettes (Fig. 4c and e) developed with inner and outer segments indicated by Rhodopsin and Peripherin-2 expression (Fig. 4d), although the degree of photoreceptor maturity might vary among rosettes as suggested by the dislocation of Rhodopsin in the cell bodies, similar to the observation in transplanted rats (Fig. 1b). L/M and S cone opsin expressions were also observed in the inner/outer segments, implying the maturation of cone photoreceptors (Fig. 4d'-d"). Contacts between PKC-positive host bipolar cells and Recoverin-positive graft photoreceptors were seen in and near the rosettes (Fig. 4e), where expressions of presynaptic Ribeye proteins and Cx36 gap junctions were found at the axonal terminals of graft photoreceptors along the host-graft interface (Fig. 4f-g). The Müller cell distribution similar to that seen in hiPSC-retinas in rats suggests there was no apparent glial boundary between the host and graft retinas (Fig. 4h). Interestingly, GFAP immunoreactivity was less evident in the graft cells possibly contacting the host retina, with an increasing gradient of GFAP immunoreactivity was found toward the distal part of the rosettes.

### 3.4. Visual field test before and after hiPSC-retina transplantation

The second monkey preparation was dedicated to visual field test to demonstrate the functional potential of transplanted hiPSC-retina in mesopic condition. A rhesus monkey was trained for monocular

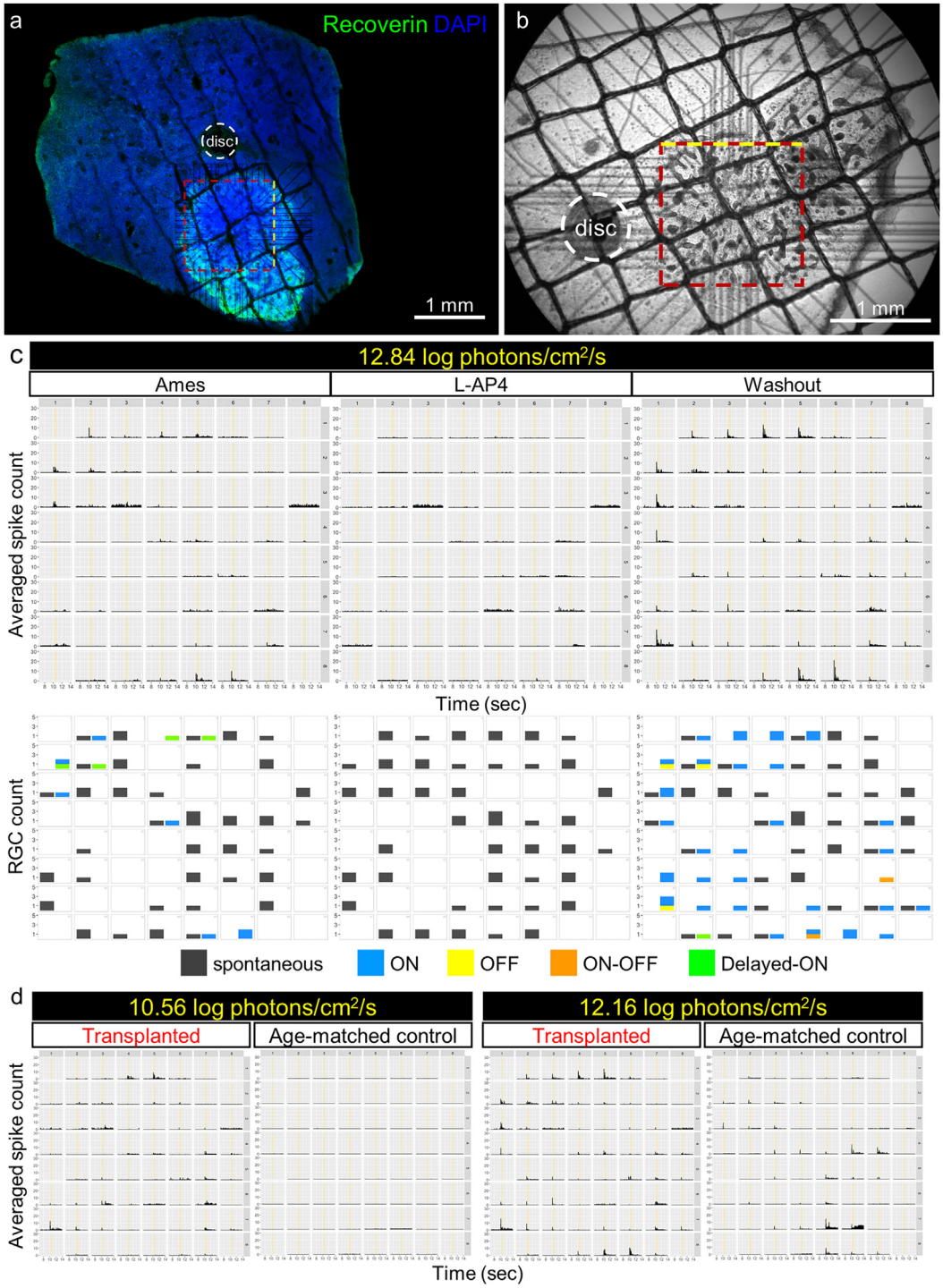


**Fig. 2.** RGC light responses detected by MEA recording in a SD-Foxn1 Tg(S334ter)3LavRrrc nude rat retina transplanted with hiPSC-retina. (a-b) An example of a 10-month-old transplanted nude rat retina mounted on MEA electrodes during recording (b) and the electrode position corresponded to the Recoverin-positive graft (a). Rosettes could be seen as dark plaques under the IR-DIC view (b). Yellow dotted lines indicate the top side of MEA electrode arrays. (c) Top row: averaged peri-stimulus time histograms (PSTH) of RGC spikes from the retina in (b) to the 1-s full-field 12.84 log photons/cm$^2$/s (presumably mesopic-to-photopic) light stimulation (indicated with yellow bars from 10 to 11 s) repeated before, during and after L-AP4 application. Bottom row: RGC numbers of each response type shown in correlation to the channel position. Note the light responses but not spontaneous firing disappeared in the presence of L-AP4 as the blocker of photoreceptor-bipolar cell synaptic transmission. No hypersensitive responses were recorded in this retina. (d) Averaged PSTH to 1-s light stimulation with lower intensities of age-matched transplanted and control nude rat retinas. RGC light responses to 10.56 log photons/cm$^2$/s (presumably scotopic-to-mesopic) were only detected in the transplanted but not in the control retina.

VGS task for the visual field mapping as described in the Materials and methods. In brief, the monkey underwent 4–8 sessions to complete a full visual field test during the one-month test period before and after photocoagulation, and 1 and 1.5 years after hiPSC-retina transplantation. Photoreceptor degeneration (ONL ablation) was induced by laser photocoagulation in 2 peri-macular regions (ROIs 1 and 2; Fig. 5a). About 2 months later, a piece of hiPSC-retina at DD59 was transplanted to the ROI 1. We confirmed by OCT imaging the presence of graft tissue at the center of degenerated region for over 2 years, which slightly expanded during the first 6 months and remained

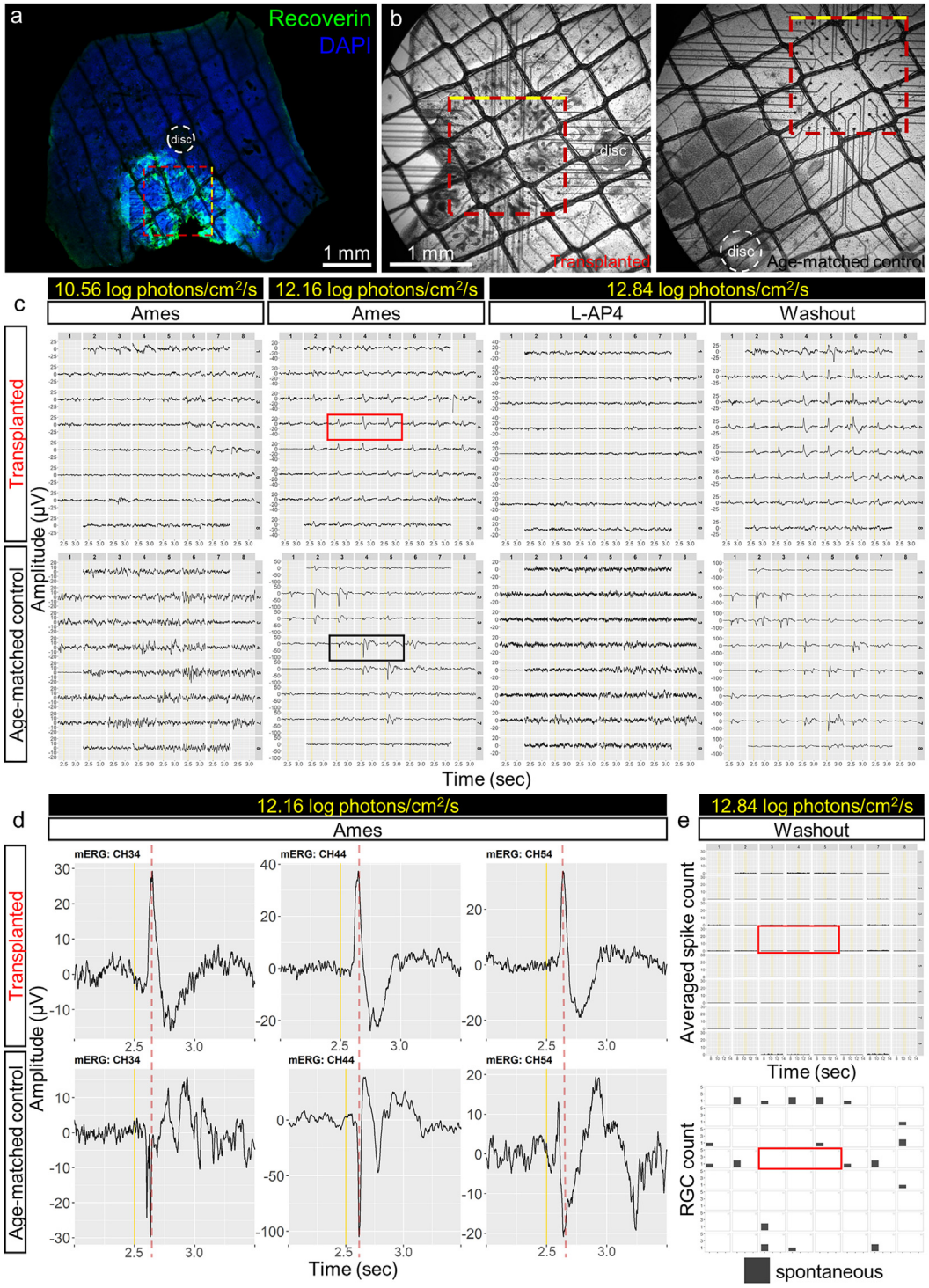


**Fig. 3.** mERG b-waves detection in a hiPSC-retinal transplanted SD-Foxn1 Tg(S334ter)3LavRrrc nude rat. (a-b) Another example of a 10-month-old transplanted nude rat retina mounted on MEA electrodes during recording (b) and the electrode position corresponded to the Recoverin-positive graft (a). Rosettes could be seen as dark plaques under the IR-DIC view (b, left) but not in the age-matched control retina (b, right). Yellow dotted lines indicate the top side of MEA electrode arrays. (c-d) Comparison of mERG recording to 10-ms full-field flash light stimulation of different light intensities in age-matched transplanted and control nude rat retinas. 1-s duration centered at the stimulation (indicated by yellow vertical lines at 2.5 s) is extracted from the 10-s recording to reveal the upward b-wave peak and downward RGC firing, if any. Note the scales of amplitude axes vary among recordings. The red- and black-boxed channels were magnified in (d) to demonstrate the upward b-wave peaks as the first response in the transplanted but not the control retina. (e) No RGC light response detection in the same transplanted retina. Note that spontaneous RGC firing was not seen in the channels (red-boxed), suggesting the graft origin of the clear mERG b-waves detected.

stable in size thereafter. Rosette-like structures inside the graft were also observed a year after transplantation (Fig. 5b and b'). Choroidal thinning or depression was observed at the transplantation site, but there was no sign of rejection as monitored by angiographies (Fig. 5c).

By VGS measurements, we were able to map the visual field with the correct saccade ratio (correct response ratios) of each target spot tested for at least 4 times per session (Fig. 5d). Considering the bias potentially resulting from the lack of attention or incorporation of the animal, the target positions were presented only if the results were valid as having enough trial numbers per day (≥ 4) and were collected both before and after transplantation. The VGS measurements before transplantation show the intensive loss of visual function in both ROIs with ONL ablation

(Fig. 5d, top-right). The visual function at the borders of both ROIs and the graft insertion site further decreased at 1 and 1.5 years post-operation, suggesting an expansion of the injured area. In contrast, a mild increase in correct VGS ratio at the transplanted site inside ROI 1 was observed but not in ROI 2 at 1.5 years after transplantation (Fig. 5d and e). In brief, of the 55 target positions in ROI 1, correct response ratio was increased in 11 positions, unchanged in 19 positions, and decreased in 25 positions while no positions were shown improved in ROI 2 – instead, they were unchanged in 26 and decreased in the other 24 positions (total 50 positions) (Fig. 5e). The superimposition of visual field map (shown in an upside-down orientation) and fundus image also suggests the visual field with improved VGS measurements was associated with the graft position. However, no evident change was detected at either ROI by focal ERG recording, while the responses at the fovea remained normal (data not shown).

### 3.5. Histology of the grafted monkey retina with potential visual function recovery

The flat-mount retina from the rhesus monkey eye tested for visual function was harvested at 26 months after transplantation for immunohistochemistry characterization. Multiple Recoverin-positive rosettes were observed within the STEM121-positive human graft (Fig. 6a-b) inside the degenerated area (ROI 1 in Fig. 5) where host photoreceptors were absent. The rosettes were mostly hemi-spherical with the photoreceptors densely packed inside and inner segments orientated centripetally, pointing to the host retinal pigment epithelium (RPE) (Fig. 6b', orthogonal views). The flat-mount tissue was further cryo-sectioned to distinguish the photoreceptors of graft-origin from the uninjured monkey photoreceptors and to reveal the detailed features of host-graft interaction (Fig. 6c-f). The graft photoreceptors were well-aligned, with their inner and outer segments orientated toward the host RPE and axonal terminals extending to the host inner retina (Fig. 6d). Furthermore, re-staining against L/M and S cone opsins and Rhodopsin revealed outer segment-like structures (Fig. 6e). Host rod bipolar cells were observed in close proximity with graft photoreceptors in both vertical sections (Fig. 6f) and reconstructed 3D projection views (Fig. 6i-j), while their axonal terminals remained organized and stratified at the bottom of the IPL (Fig. 6f). The STEM121-positive human cells were sometimes found displaced in the host INL and GCL of ROI 1 (Fig. c-f), in contrast to the ROI 2 where ONL was completely ablated and no STEM121 immunoreactivity was found (Fig. 6g-h). These observations are similar to that in both rat and monkey models after hESC-retina transplantation.

During the *in vivo* monitoring, the choroidal depression was observed by OCT in the rhesus monkey. Since we previously observed uneven RPE loss in the laser injury models [7], the choroidal atrophy may result from RPE damage. Also, considering the cyclosporine blood level remained low in this monkey (Fig. S6) but not in the other monkey that showed no apparent choroid depression, a mild local inflammatory reaction may have taken place. Still, it is noteworthy that hiPSC-retina matured and even survived long in this primate model with low immune-suppression.

## 4. Discussion

In the present study, we confirmed that hiPSC-retinas in xeno-transplantation preparation into nude rats and monkeys had a similar potency with hESC-retinas as 1) all types of human photoreceptors were observed with 2) contacts between graft photoreceptors and host bipolar cells. Furthermore, 3) host retinal light responsiveness was suggested both in the transplanted nude rat (*in vitro*) and monkey (*in vivo*) models, although conclusive discrimination of graft originated responses from remaining host cell activities was difficult to obtain with these models.

One characteristic feature of human ESC/iPSC-retinas in xeno-transplantation compared to mouse ESC/iPSC-retinas in allo-transplantation is the migration of human graft inner retinal neurons into the host inner layer indicated consistently by several human markers tested (HuNu, Ku80, STEM121), while the graft photoreceptors usually form rosettes with organized ONL structures. This may result from the relatively long period required for maturation of human ESC/iPSC-retinas after transplantation, which allows the immature inner retinal neurons of the graft to infiltrate the host inner layer, yet the interpretation of cell origins should be always dealt carefully. Moreover, at around 8 months after transplantation, the non-migrating inner neurons of the human ESC/iPSC-retinas frequently form INL/IPL-like structures surrounding the rosettes, in contrast with the graft inner neurons of mouse ESC/iPSC origin that are often expelled out of the mouse host-graft interface. This may explain the difficulty in detecting graft-driven light responses in host RGCs when compared to the allo-transplantation case. The observation of Cx36 gap junction expression at the graft photoreceptor axon terminals may suggest that transplanted human iPSC-retinas can form their inner circuitry through gap junction, besides the chemical connectivity.

Unlike *Rd1-2J* [17] or NOG-*Rd1-2J* [8] mouse models used in our previous reports, SD-Foxn1 Tg(S334ter)3LavRrrc rats had substantial light responses remained at the time of transplantation. Responsive patches were occasionally found in the mid-peripheral area of the ~10-month-old retina. These properties result in the difficulty to conclusively discriminate the graft-originated responses from the remaining sensitivity of the host retina in most of the cases. Further examination conducted at later stages or with animal models (*e.g.* NOG-*Rd1-2J*) with more advanced retinal degeneration, along with robust visual function recovery consistently observed at the grafted area, may be necessary and helpful to confirm the graft-derived responses. With the use of *NOG-Rd1-2J* model which was designed for both advanced degeneration and immunodeficiency, however, less robust responses were observed in the hESC xeno-transplantation compared to miPSC allo-transplantation in our previous report [8], suggesting that it is challenging to obtain functional evidence of neural network reconstruction by xeno neural cell therapy. After all, human clinical trials will be subsequently required to conclude the efficacy of cell-therapy approach once the safety is ensured. Interestingly, we observed the small but uniform mERG b-waves over the grafted area without RGC responses (Fig. 3). A possible explanation would be that these b-waves come from graft ON-bipolar cells, suggestive of graft light responsiveness. The lack of RGC responses, on the other hand, may be attributed to the failure of *de novo* host-graft synaptic connectivity. We have reported such occasional inconsistency between the mERG and RGC responses and suggest that the former better represents the graft functional status while the latter indicates the host-graft connectivity [8].

The hiPSC-retinas transplanted to two monkeys were well-structured and was retained for >2 years in one of them, despite the low cyclosporine blood level. Surprisingly, long-survived rosette regions correctly positioned in the host retina seem to be positively selected for survival. Although this was a single-case observation, we speculate that photoreceptors capable of forming synapses with the host might survive better, subsequently allowing the inner and outer segments of graft photoreceptors to about correct direction. Unfortunately, we could not observe the retina-RPE/choroid interface in this sample because we processed the retina for flat-mount immunostaining to align with the fundus images, but this may be relevant to the enhanced GFAP expression in the distal part of the graft photoreceptor rosettes observed in the other monkey eye.

Correspondingly with this good graft survival, a mild recovery of VGS performance was observed associated with the grafted area well over a year after transplantation. The recovery at the grafted site seemed subtle, and we could not confirm the presence of graft-origin light sensitivity by other functional examination (as discussed later). The VGS performance, however, tended to decrease on the margins of the injuries due to a possible atrophy expansion

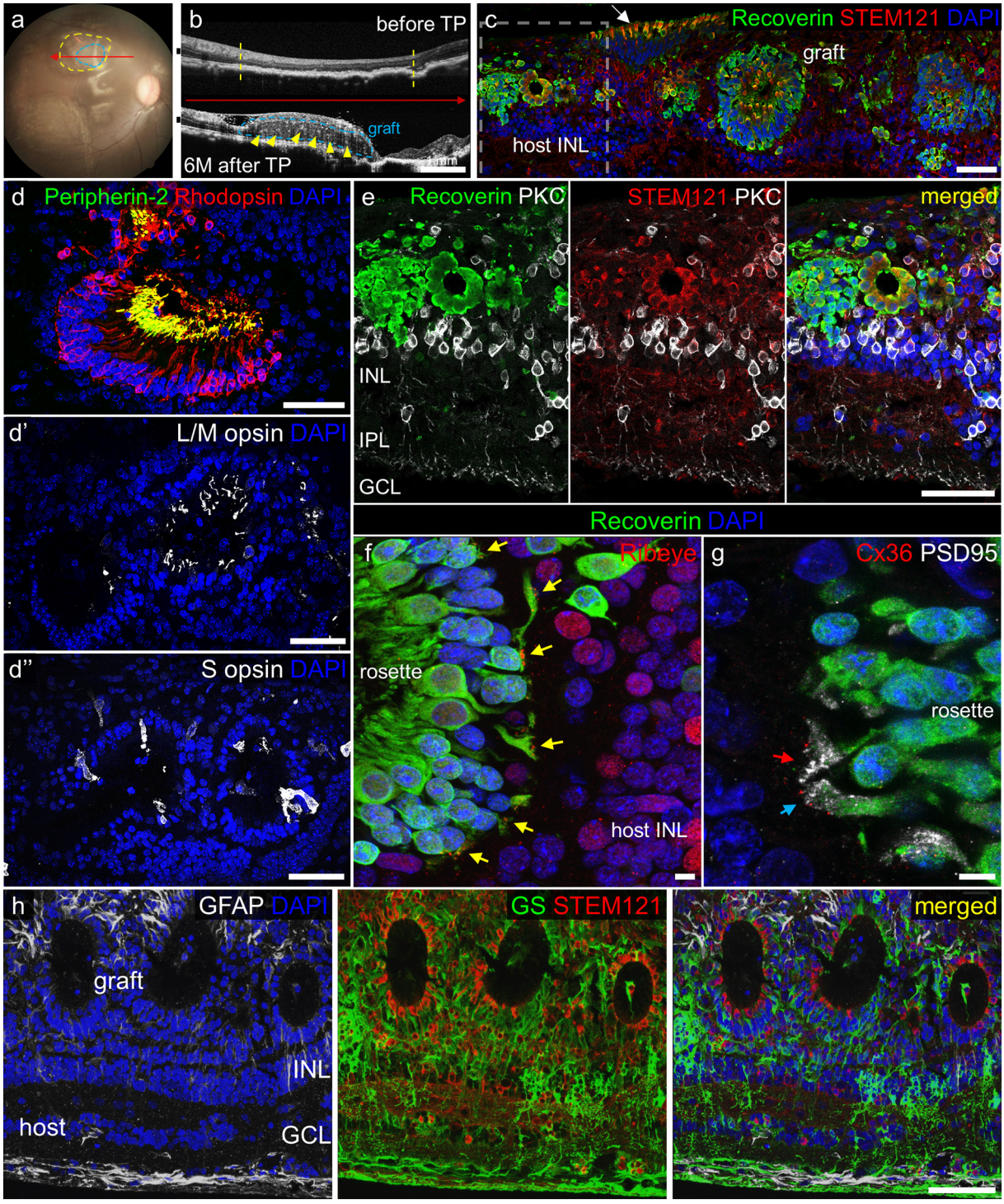


**Fig. 4.** Maturation of hiPSC-retina (~DD282) in a monkey retinal degeneration model. (a-b) *In vivo* fundus (a) and OCT (b) imaging of a cynomolgus monkey eye. ONL was focally ablated by laser photocoagulation in the area marked with the yellow dotted line, wherein the graft was placed subretinally as indicated by the blue dotted line. Red arrows indicate the position and direction of OCT imaging that demonstrates the existence of graft 6 months after transplantation with whitish rosette-like structures (yellow arrowheads). Bars at left indicate the uninjured ONL thickness. (c) Rosette formation with Recoverin-positive graft photoreceptors in the STEM121-positive transplant. The white arrow indicates where the graft photoreceptors lined up and correctly oriented toward the host RPE. (d) Maturation of graft photoreceptors with inner and outer segment formation indicated by Peripherin-2 (d) and L/M and S cone opsins (d' and d") expressions. (e) PKC-positive, STEM121-negative host bipolar cells seem to contact graft photoreceptors (positive for both Recoverin and STEM121). (f-g) Expressions of markers for ribbon synapse (f) and gap junction (g) by graft photoreceptors. Yellow arrows in (f) indicate the Ribeye expression at the photoreceptor axon terminals. Cx36 was shown expressed in (g) where the PSD95 staining indicates a neighboring pair of a cone pedicle (red arrow) and a rod spherule (blue arrow). (h) Absence of activated glial cell marker GFAP at the host-graft interface. Glutamate synthase was expressed in the Müller glia of host-graft complex, showing no glial block for graft integration in the host-graft complex. TP, transplantation; GCL, ganglion cell layer; INL, inner nuclear layer; ONL, outer nuclear layer. Scale bars equal to 1 mm (b), 50 μm (c-e, h) and 5 μm (f, g).

in both ROIs, and there were no target positions recovered inside in the ROI 2 at all. Minor increases/decreases of correct VGS outside the injuries were observed and considered pseudo-negative responses possibly due to the lack of attention of the monkey, while false-positive VGS was unlikely to occur because of the experimental nature.

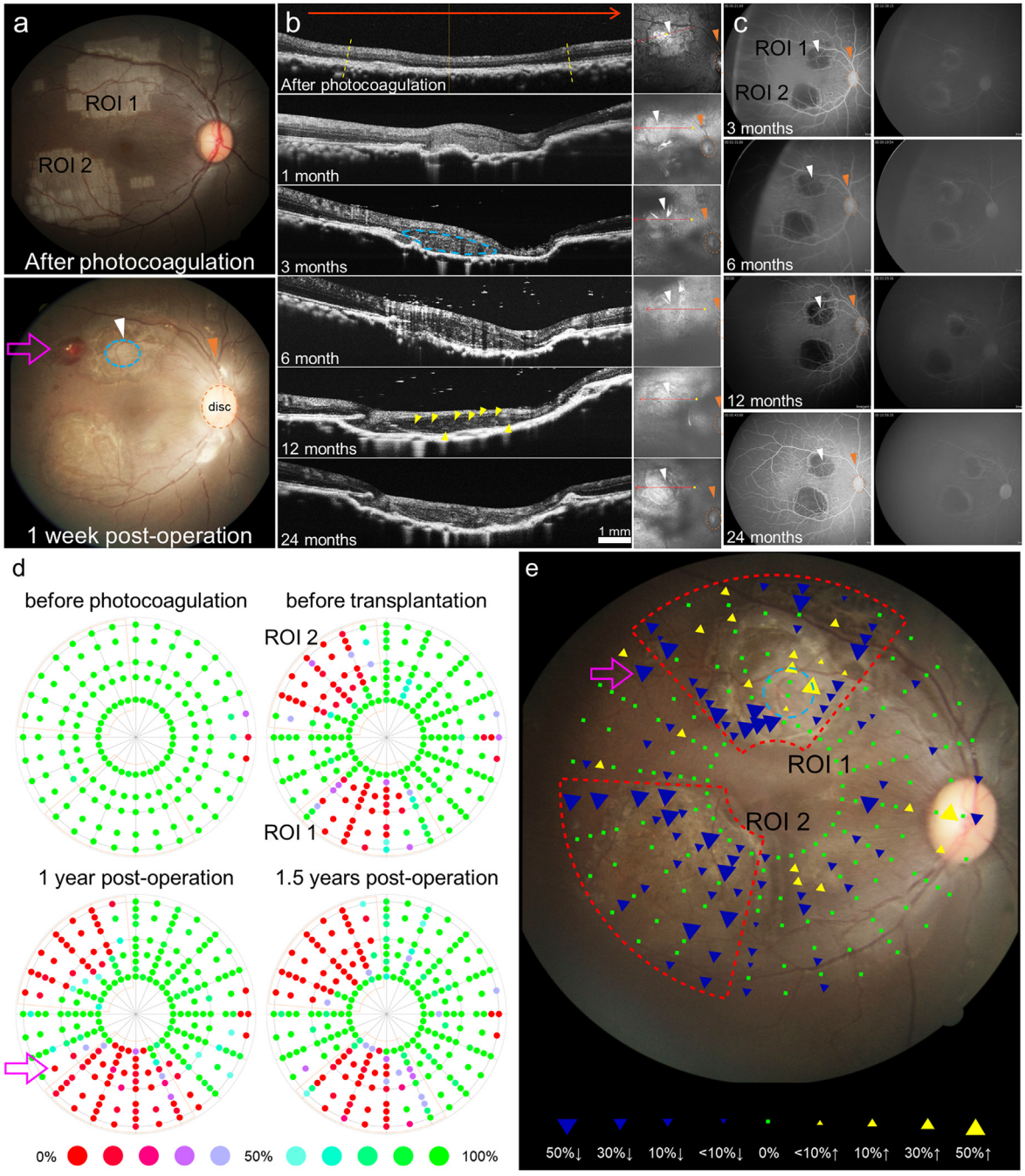


**Fig. 5.** Functional assessment of transplanted hiPSC-retina in the rhesus monkey. (a-c) *In vivo* retinal imaging of the transplanted eye. Characteristic vessel bifurcation (orange arrowheads), crossing (white arrowheads) and optic nerve discs are marked for orientation. (a) Colour fundus images at 10 days after photocoagulation (top) and 1 week after transplantation (bottom). The hiPSC-retina tissue was visible as a whitish mass (blue dotted circle). The magenta arrow indicates the entry site of hiPSC-retina during transplantation surgery. (b) OCT images of ROI 1 showing the graft survival up to 2 years after transplantation. Each panel shows the sectional view along the red arrow on the right, and rosette-like structures were seen in the graft (blue dotted line) as indicated by yellow arrowheads. (c) The FA showing no sign of rejection throughout the observation period. Left column: 1–2 min; right column: 10 min after Fluorescein injection. (d) The correct response ratio of VGS test was mapped for each target position tested for 4 times or more before photocoagulation, before transplantation, 1 and 1.5 years after transplantation, respectively. In addition to the Mariotte's blind spot at right, the two large blind areas observed in all conditions after photocoagulation corresponded to the injured ROIs 1 and 2 seen in (a). The correct response ratios are colour-coded as shown in the bottom, ranging from 0% to 100% at a step size of 10%. The magenta arrow marks the approximate surgery entry position as in panel (a). (e) Changes in correct response ratio from "before transplantation" to "1.5 years post-operation" in (d); note the results were shown in an upside-down orientation to match the fundus image wherein the graft position marked with the blue dotted circle. Target positions with improved correct response ratio were marked with yellow triangles, decreased ones with blue triangles, and unchanged ones with green squares. Surgery entry site is also marked with the magenta arrow as in panel (a). ROI, region of interest.

The lack of focal ERG detection despite the presence of VGS may be due to its lower sensitivity for end-stage degeneration as it is reportedly unable to represent the subjective vision of RP patients with the mean visual acuity of around 0.4 logMAR [27]. In fact, for evaluating the visual function during degeneration and after transplantation, assessments like *in vivo* visual field test or *in vitro* MEA recording may be of higher sensitivity and specificity than focal ERG. The former detect the output signaling of the functional retinal circuitry, even when it is composed of limited cell numbers, while the latter requires a relatively large population of retinal

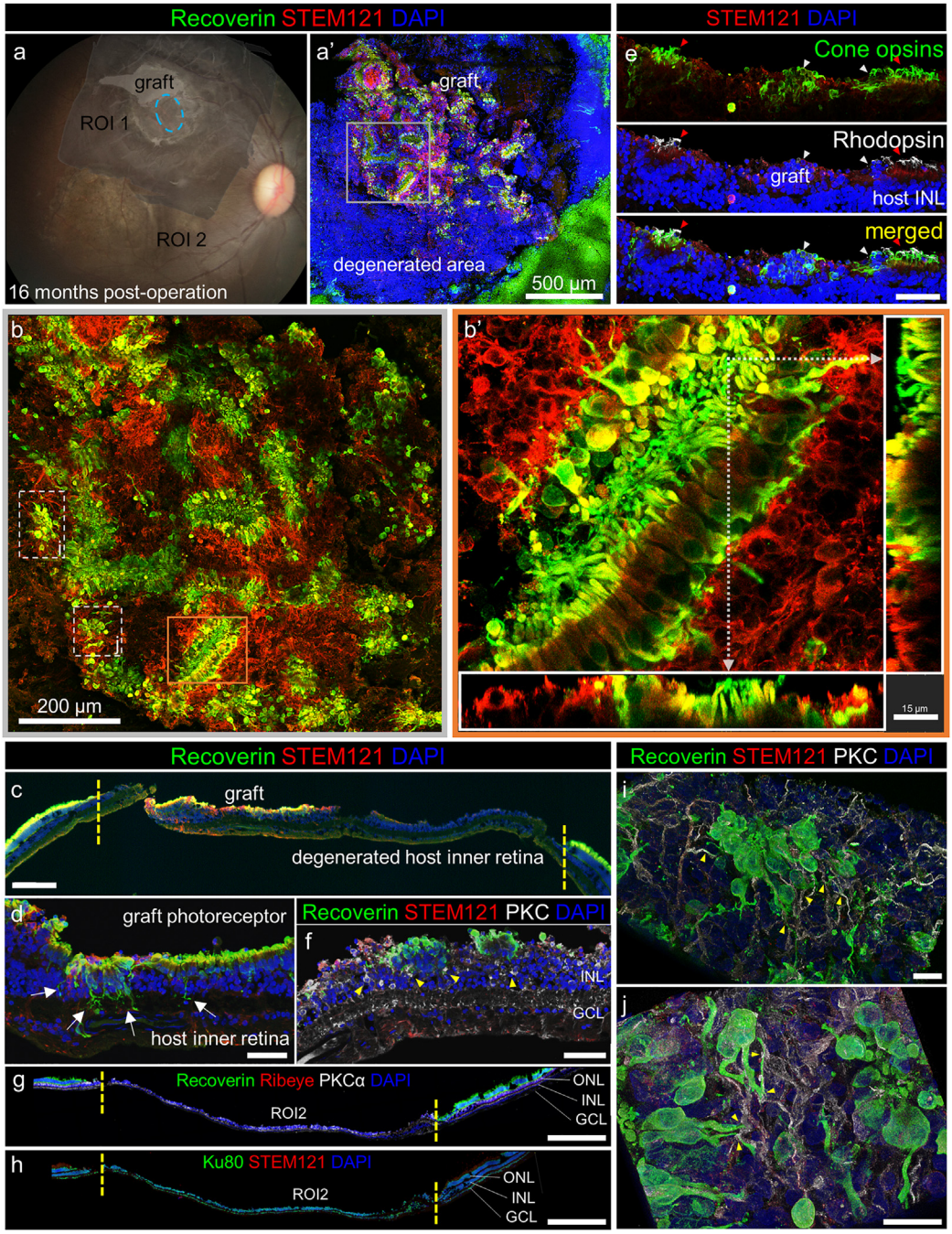


**Fig. 6.** Long-term survival and integration of hiPSC-retina in the monkey retinal degeneration model with potential functional recovery. (a-b) Flat-mount preparation of the monkey retina imaged from the RPE side to the GCL side. (a) The bright field image of the retina flat mount was merged with the colour fundus image by matching the vessel spreading to confirm the graft position (blue dotted circle). (a') Rosettes formation by Recoverin-positive graft photoreceptors inside the STEM121-positive transplant area without apparent remained host photoreceptors. Gray boxed area is magnified and shown in (b), in which the orange boxed area is further magnified and shown in (b') with the orthogonal projections demonstrating the graft photoreceptor inner segment-like structures inside the rosettes extending toward the RPE side. (c-f) Vertical sections made from the same flat mount. The STEM121 staining was confined in the degenerated region marked in between the yellow dotted lines (c). Axonal terminals of graft photoreceptors extended toward host INL, forming bulb-shaped endings indicated by white arrows (d). Maturation of both cone and rod photoreceptors with developed outer segments as indicated by red arrowheads in (e) was confirmed by re-staining of the vertical sections against L/M and S cone opsins and Rhodopsin. White arrowheads suggest where the dim staining of recoverin remained in the photoreceptor cell bodies. Yellow arrowheads in (f) indicate the potential host-graft contacts made by host rod bipolar cells with PKC but not STEM121 immunoreactivity, whose dendrites extended close to the graft photoreceptor axon terminals. (g-h) Vertical sections of the ROI 2 area showing the complete ablation of ONL between the yellow dotted lines. (g) No Recoverin-positive photoreceptors were found inside the ROI 2, while the PKCα-positive rod bipolar cells remained in the INL. Without transplantation of human tissue, the monkey cells could be labeled by Ku80 in the nuclei but not STEM121 in the cytoplasm (h). (i-j) Potential direct contacts between host rod bipolar cells and graft photoreceptors found in reconstructed z-stack images of the flat-mount preparation (yellow arrowheads). The positions of (i) and (j) in the graft are indicated in (b) with white dotted boxes. INL, inner nuclear layer; GCL, ganglion cell layer. Scale bars equal to 500 μm (a, g, h), 200 μm (b, c), 15 μm (b'), 50 μm (d-f) and 20 μm (i, j).

neurons, especially photoreceptors and bipolar cells, to respond simultaneously. This can also be supported by the detection of rat RGC light responses using MEA recording.

The use of iPSC-retina would help overcome the ethical/religious issues and enable preparation of iPSC lines of variable HLA types, which are reported to reduce the risk of rejection or prolong graft survival

[18,19]. The reduced inflammatory reaction may reciprocally enhance the regenerative process including synaptic reconstruction. Beside further study in the functional potential of iPSC-retinas, in view of clinical application, we also have several tasks to cope with, including the establishment of protocols to guarantee graft safety and quality, and optimization of surgical procedures. The graft sheet of around DD60 contains retinal progenitor cells as a majority, and the use of advanced DD graft would decrease the content of proliferative progenitor cells but also the subsequent photoreceptor cell numbers [7]. We previously reported that hESC-retinas at any development stages between DD50 and DD150 were able to fully mature after transplantation [7], and we are further optimizing the differentiation protocols and transplantation timing to obtain substantial survival/integration of photoreceptors with reduced risk. We must optimize the surgical procedures as well so as to insert multiple retinal sheets at the aimed position and orientation.

In conclusion, hiPSC-retinas behave similarly to hESC-retinas in terms of competency to mature possibly as light responsive tissues and for clinical application. The present study using the monkey model also provided an insight into how we can possibly monitor the post-operative courses of hiPSC-retina transplantation in human application. Further investigation is warranted to verify the direct host-graft connection and signal transmission in the xeno-transplantation models, and more importantly in the application for clinical trials that deal with human retinal degeneration and vision loss.

Supplementary data to this article can be found online at https://doi.org/10.1016/j.ebiom.2018.11.028.

## Acknowledgements

We thank J. Sho for help in animal experiments, M. Kawahara for support in monkey experiments, M. Horiuchi for help in immunohistochemistry, G. A. Sunagawa for advice on data analysis, Y. Kurimoto and K. Hirami for the support in monkey surgeries and all members of Takahashi lab for support and insightful discussion. We also thank the deceased Dr. Yoshiki Sasai for his great contribution to the development of hESC-retina technology.

## Funding sources

This study was supported by AMED under grant number 18bm0204002h0006. S. Yamasaki, K. Matsushita, A. Kuwahara, A. Kishino, and T. Kimura are employees of Sumitomo Dainippon Pharma; this work was supported in part by a grant from Sumitomo Dainippon Pharma.

## Declaration of Interests

The authors declare no competing interests.

## Author Contributions

M. Mandai and M. Takahashi designed and supervised the study. H.-Y. Tu conducted MEA, immunohistochemistry and data analysis. T. Watanabe and H. Shirai conducted monkey experiments and data analysis. M. Kinoshita set up and analyzed monkey visual field test. S. Yamasaki, K. Matsushita, A. Kuwahara, A. Kishino and T. Kimura prepared and characterized hiPSC-retinas. T. Hashiguchi and T. Matsuyama supported data analysis. H. Onoe supported and supervised monkey experiments. M. Eiraku, K. Suzuma, and T. Kitaoka analyzed and interpreted the data. H.-Y. Tu, T. Watanabe and M. Mandai wrote the manuscript. All authors reviewed and approved the final manuscript.

## Funding

Japan Agency for Medical Research and Development (AMED) grant (18bm0204002h0006).

## References

[1] Lamba DA, Gust J, Reh TA. Transplantation of human embryonic stem cell-derived photoreceptors restores some visual function in Crx-deficient mice. Cell Stem Cell 2009;4(1):73–9.
[2] Pearson RA, Barber AC, Rizzi M, Hippert C, Xue T, West EL, et al. Restoration of vision after transplantation of photoreceptors. Nature 2012;485(7396):99–103.
[3] Seiler MJ, Aramant RB. Cell replacement and visual restoration by retinal sheet transplants. Prog Retin Eye Res 2012;31(6):661–87.
[4] Gonzalez-Cordero A, West EL, Pearson RA, Duran Y, Carvalho LS, Chu CJ, et al. Photoreceptor precursors derived from three-dimensional embryonic stem cell cultures integrate and mature within adult degenerate retina. Nat Biotechnol 2013;31(8):741–7.
[5] Assawachananont J, Mandai M, Okamoto S, Yamada C, Eiraku M, Yonemura S, et al. Transplantation of embryonic and induced pluripotent stem cell-derived 3D retinal sheets into retinal degenerative mice. Stem Cell Rep 2014;2(5):662–74.
[6] Barnea-Cramer AO, Wang W, Lu SJ, Singh MS, Luo C, Huo H, et al. Function of human pluripotent stem cell-derived photoreceptor progenitors in blind mice. Sci Rep 2016;6:29784.
[7] Shirai H, Mandai M, Matsushita K, Kuwahara A, Yonemura S, Nakano T, et al. Transplantation of human embryonic stem cell-derived retinal tissue in two primate models of retinal degeneration. Proc Natl Acad Sci U S A 2016;113(1):E81–90.
[8] Iraha S, Tu HY, Yamasaki S, Kagawa T, Goto M, Takahashi R, et al. Establishment of immunodeficient retinal degeneration model mice and functional maturation of human ESC-derived retinal sheets after transplantation. Stem Cell Rep 2018;10(3):1059–74.
[9] Nakano T, Ando S, Takata N, Kawada M, Muguruma K, Sekiguchi K, et al. Self-formation of optic cups and storable stratified neural retina from human ESCs. Cell Stem Cell 2012;10(6):771–85.
[10] Kuwahara A, Ozone C, Nakano T, Saito K, Eiraku M, Sasai Y. Generation of a ciliary margin-like stem cell niche from self-organizing human retinal tissue. Nat Commun 2015;6:6286.
[11] Zhong X, Gutierrez C, Xue T, Hampton C, Vergara MN, Cao LH, et al. Generation of three-dimensional retinal tissue with functional photoreceptors from human iPSCs. Nat Commun 2014;5:4047.
[12] Pearson RA, Gonzalez-Cordero A, West EL, Ribeiro JR, Aghaizu N, Goh D, et al. Donor and host photoreceptors engage in material transfer following transplantation of post-mitotic photoreceptor precursors. Nat Commun 2016;7:13029.
[13] Santos-Ferreira T, Llonch S, Borsch O, Postel K, Haas J, Ader M. Retinal transplantation of photoreceptors results in donor-host cytoplasmic exchange. Nat Commun 2016;7:13028.
[14] Singh MS, Balmer J, Barnard AR, Aslam SA, Moralli D, Green CM, et al. Transplanted photoreceptor precursors transfer proteins to host photoreceptors by a mechanism of cytoplasmic fusion. Nat Commun 2016;7:13537.
[15] Hartong DT, Berson EL, Dryja TP. Retinitis pigmentosa. Lancet 2006;368(9549):1795–809.
[16] Punzo C, Kornacker K, Cepko CL. Stimulation of the insulin/mTOR pathway delays cone death in a mouse model of retinitis pigmentosa. Nat Neurosci 2009;12(1):44–52.
[17] Mandai M, Fujii M, Hashiguchi T, Sunagawa GA, Ito SI, Sun J, et al. iPSC-derived retina transplants improve vision in rd1 end-stage retinal-degeneration mice. Stem Cell Rep 2017;8(1):69–83.
[18] Morizane A, Kikuchi T, Hayashi T, Mizuma H, Takara S, Doi H, et al. MHC matching improves engraftment of iPSC-derived neurons in non-human primates. Nat Commun 2017;8(1):385.
[19] Sugita S, Iwasaki Y, Makabe K, Kimura T, Futagami T, Suegami S, et al. Lack of T cell response to iPSC-derived retinal pigment epithelial cells from HLA homozygous donors. Stem Cell Rep 2016;7(4):619–34.
[20] Seiler MJ, Aramant RB, Jones MK, Ferguson DL, Bryda EC, Keirstead HS. A new immunodeficient pigmented retinal degenerate rat strain to study transplantation of human cells without immunosuppression. Graefes Arch Clin Exp Ophthalmol 2014;252(7):1079–92.
[21] Nakagawa M, Taniguchi Y, Senda S, Takizawa N, Ichisaka T, Asano K, et al. A novel efficient feeder-free culture system for the derivation of human induced pluripotent stem cells. Sci Rep 2014;4:3594.
[22] Murakami I, Komatsu H, Kinoshita M. Perceptual filling-in at the scotoma following a monocular retinal lesion in the monkey. Vis Neurosci 1997;14(1):89–101.
[23] Takakuwa N, Kato R, Redgrave P, Isa T. Emergence of visually-evoked reward expectation signals in dopamine neurons via the superior colliculus in V1 lesioned monkeys. Elife 2017;6.
[24] Mandai M, Homma K, Okamoto S, Yamada C, Nomori A, Takahashi M. Adequate time window and environmental factors supporting retinal graft cell survival in rd mice. Cell Med 2012;4(1):45–54.
[25] Bloomfield SA, Volgyi B. The diverse functional roles and regulation of neuronal gap junctions in the retina. Nat Rev Neurosci 2009;10(7):495–506.
[26] Martinez-Navarrete G, Seiler MJ, Aramant RB, Fernandez-Sanchez L, Pinilla I, Cuenca N. Retinal degeneration in two lines of transgenic S334ter rats. Exp Eye Res 2011;92(3):227–37.
[27] Oishi A, Nakamura H, Tatsumi I, Sasahara M, Kojima H, Kurimoto M, et al. Optical coherence tomographic pattern and focal electroretinogram in patients with retinitis pigmentosa. Eye (Lond) 2009;23(2):299–303.